ChemComm

COMMUNICATION

View Article Online
View Journal | View Issue

Published on 30 May 2019. Downloaded by State University of New York at Albany on 8/29/2019 10:21:11 PM.

Check for updates

Cite this: *Chem. Commun.*, 2019, **55**, 7243

Received 12th April 2019,
Accepted 30th May 2019

DOI: 10.1039/c9cc02836f

rsc.li/chemcomm

From lithium to sodium: design of heterometallic molecular precursors for the $NaMO_2$ cathode materials†

Haixiang Han,[ab] Zheng Zhou,[a] Jesse C. Carozza,[a] Jeff Lengyel,[c] Yuan Yao,[b] Zheng Wei[a] and Evgeny V. Dikarev*[a]

Based on the well-established model structure of $Li_2M_2(tbaoac)_6$, the first series of heterometallic molecular precursors $Na_2M_2(tbaoac)_6(THF)_2$ (M = Fe, Co, and Ni) have been designed and successfully utilized for the preparation of $NaMO_2$ oxide cathode materials of sodium-ion batteries.

Sodium-ion battery (SIB) cathodes are of great interest to supplement the now-ubiquitous lithium (LIB) analogues, especially for large-scale applications, due to sodium's natural abundance and competitive electrochemistry.[1–3] It is well-established that the larger ionic radius of Na^+ severely limits the number of viable host structures that allow for reversible sodium de/intercalation. The layered sodium-transition metal oxides $NaMO_2$ represent one of the most promising hosts by providing comparable activity to canonical LIBs.[3] This class of compounds can be divided into two major groups, O3 and P2, based on the location of sodium ions at either octahedral or prismatic sites, respectively, squeezed in between the edge-sharing sheets of $[MO_6]$ octahedra.[4] Current efforts to improve the electrochemical properties of these layered oxides are primarily focused on formation of nanoparticles with highly homogenous metal/vacancy distribution,[5] and therefore, are intimately tied up to the choice of synthetic strategy.[1]

Presently, SIB cathode material preparation is dominated by ball-milling solid state reactions, co-precipitation, sol–gel, and multi-source precursor techniques, which employ physically/chemically incompatible starting reagents that often cause inhomogeneous metal distribution within the target oxide.[6–10] Furthermore, the high temperatures required for annealing of these mixtures often result in nanoparticles sintering and agglomerating into larger aggregations, destroying the unique properties brought in by small particle size and specific morphology of materials.[3,11–13]

The single-source precursor (SSP) approach is the best way to address the above issues as it utilizes molecular complexes containing all necessary elements in the proper ratio and offering low-temperature decomposition pathways to the target functional materials.[14,15] The intimate mixing of the key elements at the molecular level also provides for a rapid interaction within the heterometallic assembly, effectively preventing the formation of undesired, thermally-stable intermediates.[16] At the same time, the major challenge for the SSP approach remains the design of a suitable molecular complex that features required stoichiometry, clean decomposition pattern, and high solubility in common solvents, while retaining heterometallic structure in solution.[17] Recently-suggested precursors for the Na : M = 1 : 1 layered oxide materials all have polymeric structures $[NaML_3]_\infty$ (L = acac,[5] hfac[13]). These compounds are insoluble in non-coordinating solvents, while readily dissociating into homometallic fragments in coordinating ones. Such properties effectively limit precursor feasibility for a number of advanced application techniques, *i.e.*, liquid injection, which is well-known to afford oxide materials in the form of nanoparticles or thin films.

We have previously developed an effective unsymmetric ligand approach to design molecular precursors $Li_2M_2L_6$ (Scheme 1a; M = transition metal) for the low-temperature preparation of $LiMO_2$ cathode materials.[15–17] The unsymmetric groups used in the above design feature different (small/bulky) substituents at the two ligand ends. Only the ligand oxygen near the small group is able to participate in both chelating and bridging interactions, while the oxygen under the bulky, sterically-congested end remains purely chelating. The employment of such unsymmetric ligands is effectively changing the connectivity pattern within the heterometallic assembly, allowing

[a] *Department of Chemistry, University at Albany, State University of New York, 1400 Washington Ave., Albany, NY 12222, USA. E-mail: edikarev@albany.edu*
[b] *Department of Materials Science and Engineering, Cornell University, NY 14850, USA*
[c] *Department of Chemistry and Biochemistry, Florida State University, FL 32306, USA*

† Electronic supplementary information (ESI) available: Synthetic details, characterization procedures, X-ray powder diffraction patterns, IR and mass spectra, phase analysis of thermal decomposition traces of heterometallic precursors. CCDC 1904470–1904473. For ESI and crystallographic data in CIF or other electronic format see DOI: 10.1039/c9cc02836f

Published on 30 May 2019. Downloaded by State University of New York at Albany on 8/29/2019 10:21:11 PM.

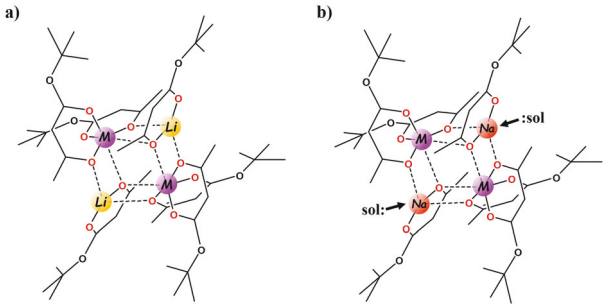

Scheme 1 Design of Na : M = 1 : 1 molecular precursor based on the model structure of Li analogue.

for the formation of compounds with discrete molecular structures.[17] Among several unsymmetric ligands employed, tbaoac (*tert*-butyl acetoacetate) exhibits superior properties such as the lowest decomposition temperature leading to the phase-pure target product as well as the miniscule contribution of the ligand cost to the target material production, thus making the above SSP approach attractive for large-scale applications.[17]

The tetranuclear structure of $Li_2M_2(tbaoac)_6$ depicted in the Scheme 1a contains tetrahedrally-coordinated Li ions.[16–18] Based on our prior experience, such a model is unlikely suitable for the analogous sodium-containing complex, since Na ion usually commands higher coordination numbers of five or six. We envisaged that it would require an additional neutral donor ligand to satisfy the Na coordination environment (Scheme 1b). Herein, we employ the unsymmetric, inexpensive tbaoac ligand along with the strong O-donor THF to design the first family of heterometallic Na : M = 1 : 1 molecular precursors $Na_2M_2(tbaoac)_6(THF)_2$.

The heterometallic precursors $Na_2M_2(tbaoac)_6(THF)_2$ (M = Fe (**1**), Co (**2**), Ni (**3**), Mg (**4**)) have been prepared in coordinating solvents on a large scale, in nearly quantitative yield using commercially/readily available starting reagents through the following synthetic procedures performed at room temperature (see ESI† for more details):

$$6Na(tbaoac) + 2MCl_2 + 2THF \rightarrow Na_2M_2(tbaoac)_6(THF)_2 + 4NaCl \quad (1)$$

$$2Na(tbaoac) + 2M(tbaoac)_2 + 2THF \rightarrow Na_2M_2(tbaoac)_6(THF)_2 \quad (2)$$

The reactions (1) and (2) were performed in THF, which acts as both reagent and reaction medium. Even though method (2) yields $Na_2M_2(tbaoac)_6(THF)_2$ as a sole product, it requires prior preparation of $M(tbaoac)_2$ as an extra step.

Heterometallic precursors **1–4** appear as fine powders in the colors of orange, pink, green, and white, respectively. Compounds **1** and **2** are relatively sensitive in solution, with air-exposure resulting in a color change to dark-red and green, respectively, indicating the oxidation of divalent iron and cobalt. At the same time, **1** and **2** are stable in the solid state for a reasonable period of time. Compounds **3** and **4** are stable in both solution and the solid state. Heterometallic precursors are soluble in all common solvents. The dissociation of THF

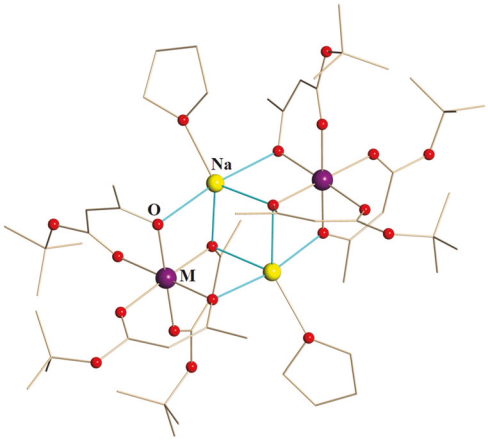

Fig. 1 Molecular structure of $Na_2M_2(tbaoac)_6(THF)_2$ (M = Fe, Co, Ni, Mg; Δ-,Δ-enantiomer). The sodium–oxygen bonds to the tbaoac ligands involved in the bridging interactions are shown in blue. Hydrogen atoms are omitted for clarity. The structural views with thermal ellipsoids can be found in Fig. S5–S8 (ESI†).

from **1–4** takes place at the temperatures above 60 °C, accompanied by a dramatic change in their powder X-ray diffraction patterns.

Single crystal X-ray diffraction analysis revealed that precursors **1–4** are all isomorphous and crystallize in the centrosymmetric triclinic crystal system. The crystal structure consists of tetranuclear heterometallic molecules (Fig. 1) with Na : M ratio of 1 : 1. Two transition metal centers bear three chelating tbaoac ligands each, exhibiting a distorted octahedral coordination environment. The sodium centers are 5-coordinate with four bridging oxygens coming from the tbaoac ligands and one from THF molecule. Molecular structures **1–4** feature six bulky O^{t}Bu groups facing outward of heterometallic assembly and, along with two THFs, providing a screening protection for the metal cores from being engaged in intermolecular interactions that could result in oligomerization and formation of polymeric chains. The averaged metal–oxygen bond lengths in the structures of heterometallic precursors **1–4** (Table 1) show a trend that corresponds well with the radii of divalent Fe, Co, Ni, and Mg ions. While the chelating–bridging M–O distances appear to be somewhat shorter than the chelating ones, a similar situation has been observed previously for the $Li_2M_2(tbaoac)_6$ system.[16]

Despite certain compositional and structural similarities between the two families of heterometallic precursors $Li_2M_2(tbaoac)_6$

Table 1 Averaged metal–oxygen bond lengths (Å) in the structures of heterometallic precursors **1–4** (L = tbaoac). The full list of bond distances and angles can be found in Tables S10–S13 (ESI)

	M–O$_c$[a]	M–O$_{c–b}$[b]	Na–O$_b$[c]	Na–O$_{THF}$
$Na_2Fe_2L_6(THF)_2$ (**1**)	2.103(1)	2.084(1)	2.361(2)	2.358(2)
$Na_2Co_2L_6(THF)_2$ (**2**)	2.072(1)	2.061(1)	2.351(2)	2.356(2)
$Na_2Ni_2L_6(THF)_2$ (**3**)	2.038(1)	2.031(1)	2.351(2)	2.357(2)
$Na_2Mg_2L_6(THF)_2$ (**4**)	2.051(2)	2.051(2)	2.366(2)	2.360(2)

[a] c – chelating. [b] c–b – chelating–bridging. [c] c – bridging.

 This journal is © The Royal Society of Chemistry 2019

Published on 30 May 2019. Downloaded by State University of New York at Albany on 8/29/2019 10:21:11 PM.

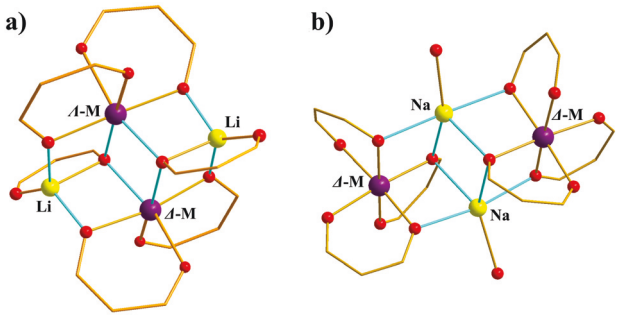

Fig. 2 Tetranuclear cores $[A_2M_2L_6]$ (A = Li (a) and Na (b); L = tbaoac) representing different connectivity patterns within heterometallic assemblies as well as different chiralities of transition metal centers.

and $Na_2M_2(tbaoac)_6(THF)_2$, they appear to be different in many aspects. Specifically, the latter is featuring 5-coordinated alkali metals in addition to all ligands chelating transition metal ions. That results in distinctively different heterometallic tetranuclear cores as shown in Fig. 2. Another notable difference is that $Li_2M_2(tbaoac)_6$ molecule (Fig. 2a) has an inversion center in the middle of heterometallic assembly, making two transition metal centers to display the opposite Δ/Λ-chiralities. Conversely, the $Na_2M_2(tbaoac)_6$ core (Fig. 2b) does not contain any extra crystallographic symmetry and features its transition metals in either Δ,Δ- or Λ,Λ-configurations. However vaguely, the latter represents an alternative connectivity pattern within the tetranuclear cyclic assembly by which a diastereomer to the lithium counterpart can be constructed.

The ^{1}H NMR investigation of compounds **1–3** in chloroform, acetone, and THF revealed signal-silent spectra, indirectly confirming the retention of heterometallic structures in solution. The diamagnetic analog $Na_2Mg_2(tbaoac)_6(THF)_2$ (**4**) has been specifically isolated to assess the solution behavior of heterometallic core by NMR spectroscopy. The ^{1}H NMR spectrum of **4** in chloroform displays three singlets that correspond to tbaoac ligand protons in addition to two signals of coordinated THF molecules (Fig. 3; Fig. S13 and Table S14, ESI†), thus confirming that heterometallic structure remains intact upon dissolution.

The ''gas-phase structure'' of heterometallic precursors **1–3** has been investigated by Direct Analysis in Real Time (DART)

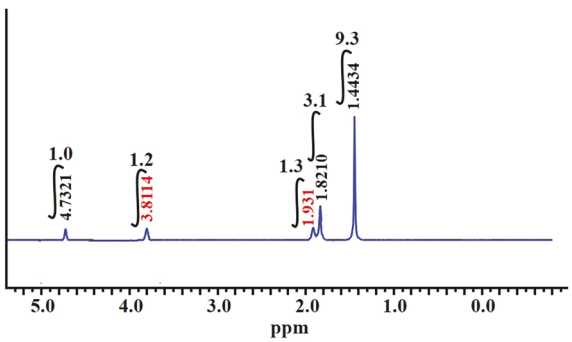

Fig. 3 ^{1}H NMR spectrum of heterometallic precursor $Na_2Mg_2(tbaoac)_6(THF)_2$ (**4**) in $CDCl_3$ recorded at room temperature.

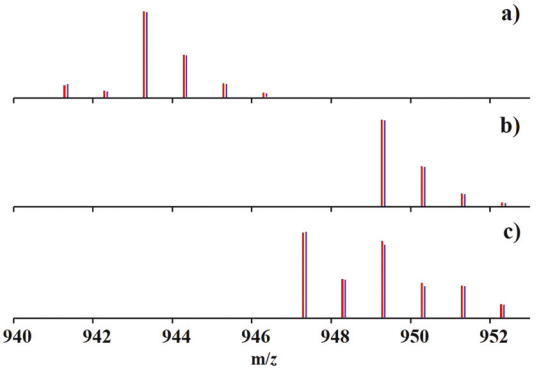

Fig. 4 Isotope distribution patterns for the $[M–L]^+$ (L = tbaoac) ion in positive ion DART mass spectra of precursors **1–3**: (a) $[Na_2Fe_2(tbaoac)_5(THF)_2]^+$, (b) $[Na_2Co_2(tbaoac)_5(THF)_2]^+$ and (c) $[Na_2Ni_2(tbaoac)_5(THF)_2]^+$. The blue and red lines are experimental and simulated patterns, respectively. Full analysis of mass spectra as well as the data for complex **4** can be found in Fig. S14–S17 and Tables S15–S26 (ESI†).

mass spectrometry, which was previously shown[15,16,18] as very effective for the task due to its soft ionization process. In the positive ion spectra, the presence of the $[M–L]^+$ ions (L = tbaoac) for all molecular precursors was unambiguously confirmed along with their corresponding characteristic isotope distribution patterns (Fig. 4). Noteworthy is the observation that the $[M–L–2THF]^+$ species have also been detected, indicating the retention of heterometallic core with a proper Na : M = 1 : 1 ratio in the gas phase even upon dissociation of THF molecules (Fig. S14–S17, ESI†).

Understanding the thermal behavior of heterometallic precursors is greatly important for the preparation of target oxide materials by thermal decomposition. Thermogravimetric analysis (TGA) of molecular precursor $Na_2Fe_2(tbaoac)_6(THF)_2$ (**1**) was carried out in the air to corroborate the visual and thermodiffraction observations of its behavior upon heating (Fig. S18, ESI†). The obvious degradation of compound **1** starts at 50–60 °C and is related to the departure of THF molecules. A fast weight loss takes place between 128–132 °C and gradually ends at *ca.* 400 °C. The total weight loss at this point is 81.3%, which corresponds well to the theoretical value of 82.2% for the formation of stoichiometric target oxide $NaFeO_2$. The next weight loss occurs above 700 °C and is attributed to the slow evaporation of sodium in the form of oxide/peroxide. The total weight loss (88.3%) measured at 800 °C may indicate the formation of Fe_2O_3 with a theoretical residue value of 87.2%.

Thermal decomposition of heterometallic single-source precursors **1–3** results in phase-pure oxides, which represent prospective cathode materials for the sodium-ion batteries. Specifically, phase-pure O′3-type $NaNiO_2$ was obtained through thermal decomposition of $Na_2Ni_2(tbaoac)_6(THF)_2$ (**3**) at 600 °C (Fig. 5a, Fig. S23 and Table S31, ESI†), while single-source precursors $Na_2Fe_2(tbaoac)_6(THF)_2$ (**1**) and $Na_2Co_2(tbaoac)_6(THF)_2$ (**2**) demonstrate versatility in preparation of different phases upon thermolysis at different temperatures/conditions (Fig. 5b and c). Low-temperature decomposition (450 °C) of $Na_2Fe_2(tbaoac)_6(THF)_2$ (**1**) in O_2 atmosphere results in stoichiometric α(O3)-$NaFeO_2$

Published on 30 May 2019. Downloaded by State University of New York at Albany on 8/29/2019 10:21:11 PM.

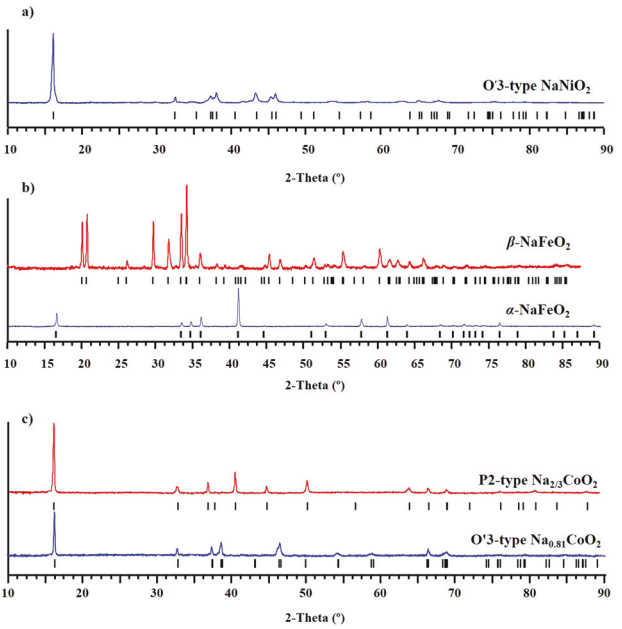

Fig. 5 X-ray powder diffraction patterns of (a) O′3-type of $NaNiO_2$, (b) α(O3)- and β-types of $NaFeO_2$, and (c) O′3- and P2-types of Na_xCoO_2 oxides obtained by thermal decomposition of respective single-source precursors under different conditions.

phase, while treatment of **1** at 500 °C in air leads to a different polymorph, namely β-$NaFeO_2$ (Fig. 5b, Fig. S19 and S20, Tables S27 and S28, ESI†). Thermal decomposition of $Na_2Co_2(tbaoac)_6(THF)_2$ (**2**) at relatively low-temperature (450 °C) yields O′3-Na_xCoO_2 phase, while elevating temperature to 750 °C gives rise to the P2-type of Na_xCoO_2 oxide (Fig. 5c, Fig. S21 and S22, Tables S29 and S30, ESI†). Apparently, the thermolysis of compound **2** is accompanied by the gradual loss of sodium *via* its sublimation in the form of oxide/peroxide, which is a common phenomenon in the preparation of sodium–cobalt oxides.[5] ICP analysis confirmed the Na:Co ratios in decomposition products as 0.81 and 0.70 for the O′3 and P2 forms, respectively, that corresponds well to the structural characteristics obtained by X-ray powder diffraction technique. Transmission electron microscopy (TEM) of P2-Na_xCoO_2 oxide obtained by thermal decomposition of molecular precursor **2** revealed the particles size in the range of 60–130 nm (Fig. S24a, ESI†). The circular voltammetry and galvanostatic discharge behavior of this material has been briefly investigated. With Ag and Pt wires as the reference and counter electrodes, the P2-Na_xCoO_2 oxide is active within the potential range of −1.5 to 0.5 V (Fig. S24b, ESI†) and the discharge capacities in the first two cycles reaching up to 124 and 128 mA h g^{-1} (Fig. S24c, ESI†), respectively, which are superior to most of the data reported so far.[1,3] However, a severe capacity fading starts afterward. This may be ascribed to the particle pulverization resulting from sodium ion intercalation during the first two reaction cycles.

In conclusion, the first series of heterometallic molecular precursors $Na_2M_2(tbaoac)_6(THF)_2$ were obtained. They all exhibit isomorphous tetranuclear structures with the Na : M ratio of 1 : 1 and demonstrate clean decomposition patterns to yield phase-pure sodium-transition metal oxides, which belong to an important class of cathode materials for sodium-ion batteries. In addition to this application, the reported tetranuclear structure can be employed as a model for further design of heterotrimetallic $Na_2MM'(tbaoac)_6(THF)_2$ molecular precursors featuring two different 3d transition metal ions.

This work was financially supported by the National Science Foundation (CHE-1152441).

Conflicts of interest

There are no conflicts to declare.

Notes and references

1 N. Yabuuchi, K. Kubota, M. Dahbi and S. Komaba, *Chem. Rev.*, 2014, **114**, 11636–11682.
2 N. Yabuuchi and S. Komaba, *Sci. Technol. Adv. Mater.*, 2014, **15**, 043501.
3 J.-Y. Hwang, S.-T. Myung and Y.-K. Sun, *Chem. Soc. Rev.*, 2017, **46**, 3529–3614.
4 C. Delmas, C. Fouassier and P. Hagenmuller, *Physica B+C*, 1980, **99**, 81–85.
5 M. Li, K. Yang, J. Liu, X. Hu, D. Kong, T. Liu, M. Zhang and F. Pan, *Chem. Commun.*, 2018, **54**, 10714–10717.
6 X. Ma, H. Chen and G. Ceder, *J. Electrochem. Soc.*, 2011, **158**, A1307–A1312.
7 N. K. Samin, R. Rusdi, N. Kamarudin and N. Kamarulzaman, *Adv. Mater. Res.*, 2012, **545**, 185–189.
8 P. Vassilaras, X. Ma, X. Li and G. Ceder, *J. Electrochem. Soc.*, 2013, **160**, A207–A211.
9 X. Wang, M. Tamaru, M. Okubo and A. Yamada, *J. Phys. Chem. C*, 2013, **117**, 15545–15551.
10 J. Billaud, R. J. Clément, A. R. Armstrong, J. Canales-Vázquez, P. Rozier, C. P. Grey and P. G. Bruce, *J. Am. Chem. Soc.*, 2014, **136**, 17243–17248.
11 S. Hildebrandt, A. Eva, P. Komissinskiy, C. Fasel, I. Fritsch and L. Alff, *J. Sol–Gel Sci. Technol.*, 2012, **63**, 307–314.
12 T. Kodera and T. Ogihara, *J. Ceram. Soc. Jpn.*, 2014, **122**, 483–487.
13 J. Zhao, J. Xu, D. H. Lee, N. Dimov, Y. S. Meng and S. Okada, *J. Power Sources*, 2014, **264**, 235–239.
14 A. Navulla, L. Huynh, Z. Wei, A. S. Filatov and E. V. Dikarev, *J. Am. Chem. Soc.*, 2012, **134**, 5762–5765.
15 H. Han, Z. Wei, M. C. Barry, A. S. Filatov and E. V. Dikarev, *Dalton Trans.*, 2017, **46**, 5644–5649.
16 H. Han, Z. Wei, M. C. Barry, J. C. Carozza, M. Alkan, A. Y. Rogachev, A. S. Filatov, A. M. Abakumov and E. V. Dikarev, *Chem. Sci.*, 2018, **9**, 4736–4745.
17 Z. Wei, H. Han, A. S. Filatov and E. V. Dikarev, *Chem. Sci.*, 2014, **5**, 813–818.
18 H. Han, Z. Wei, A. S. Filatov, J. C. Carozza, M. Alkan, A. Y. Rogachev, A. Shevtsov, A. M. Abakumov, C. Pak, M. Shatruk, Y.-S. Chen and E. V. Dikarev, *Chem. Sci.*, 2019, **10**, 524–534.

 This journal is © The Royal Society of Chemistry 2019